Electronic Supplementary Information

A cationic $[Ag_{12}S_{12}]$ cluster-based 2D coordination polymer and its dye composite with enhanced photocurrent and dielectric responses

Min Zhang,[a] Yu-Ling Tan,[a] Xu-Ran Chen,[a] Hong Yu,*[a] Wen-Hua Zhang,*[a] and Jian-Ping Lang*[ab]

[a]College of Chemistry, Chemical Engineering and Materials Science, Soochow University, Suzhou 215123, Jiangsu, People's Republic of China

[b]State Key Laboratory of Organometallic Chemistry, Shanghai Institute of Organic Chemistry, Chinese Academy of Sciences, Shanghai 200032, People's Republic of China

Contents

Experimental section

General procedures. $TabHPF_6$ was prepared according to the literature method.[S1] All the other chemicals and solvents were commercially available and used without further purification. The elemental analyses (EA) of C, H, N, and S were carried out on a Vario Micro cube organic elemental analyzer. Fourier transform infrared (FT-IR) spectra were obtained using a Thermo Electron NEXUS 670 FT-IR spectrometer (KBr disks, 4000–400 cm^{-1}). The ^1H NMR spectra were recorded on a Varian UNITY Plus-400 spectrometer at ambient temperature. Thermogravimetric analyses (TGA) were performed on a Mettler TGA/SDTA851 thermal analyzer from room temperature to 800 ºC, at a heating rate of 10 ºC min^{-1} under an N_2 atmosphere. The powder X-ray diffraction (PXRD) patterns were collected with a PANalytical Aeris diffractometer (Cu-Kα). The concentration of Ag^+ in aqueous solutions were determined by inductively coupled plasma atomic emission spectrometry (ICP-AES) using a Varian 710-ES ICP atomic emission spectrometer. The UV-Vis spectra and optical diffuse reflectance spectra were obtained with a Shimadzu UV-2600 spectrometer. The sorption isotherms of N_2 were measured by a Belsorp surface area and porosity analysis instrument at 77 K, with the Brunauer-Emmett-Teller (BET) method utilized to calculate the specific surface area. Zeta potential of **2a**, **3**, and CR were recorded on a Malvern Zetasizer Nano ZS instrument. The X-ray photoelectron spectra (XPS) were collected with an ESCALAB 250Xi spectrometer. Energy dispersive X-ray (EDX) spectra were obtained from a Carl Zeiss EVO 18 scanning electron microscope. Photocurrent response measurements were performed on a CHI 660E electrochemistry workstation. The dielectric properties were examined on a Novocontrol Concept 80 broadband dielectric spectrometer.

Preparation of $[Ag_6(Tab)_6(Bpee)_2(MeCN)]_2(PF_6)_{12}\cdot 6DMF\cdot 2MeCN$ (2). AgOAc (0.45 mmol, 75.1 mg) and $TabHPF_6$ (0.45 mmol, 140.9 mg) were mixed and grinded for *ca* 30 min at room temperature. Upon grinding, the white mixture gradually turned yellow, accompanied by a smell of acetic acid. Subsequently, Bpee (0.15 mmol, 27.3 mg) was introduced and the mixture further ground for *ca* 30 min. The yellow powder was then dissolved in a mixture of MeCN (5 mL) and DMF (5 mL) to yield a yellow solution that was subjected to slow Et_2O diffusion. Faint yellow block crystals of **2** were obtained after two weeks, which were collected and washed with Et_2O. The coordinated and free MeCN, as well as part of the lattice DMF solvents, were found to readily escape from the crystals at ambient temperature. The following data are thus based on the formula of $[Ag_6(Tab)_6(Bpee)_2]_2(PF_6)_{12}\cdot 4DMF$ (**2a**). Yield: 148.1 mg (62.5%). Anal. Calcd (%) for $C_{168}H_{224}Ag_{12}F_{72}N_{24}O_4P_{12}S_{12}$: C, 33.28; H, 3.72; N, 5.55; S, 6.35. Found: C, 32.76; H, 3.66; N,

5.61; S, 6.43. IR (KBr disk, cm^{-1}): 1660 (m), 1604 (m), 1489 (s), 1419 (w), 1385 (w), 1124 (m), 1010 (m), 959 (w), 840 (s), 744 (m), 558 (s). ^{1}H NMR (400 MHz，DMSO-d_6, ppm): 8.59−8.60 (d, J = 5.1 Hz, 8H in py), 7.95 (s, CHO in DMF), 7.54−7.68 (m, 36H, 4H in CH of Bpee + 24H in Ph + 8H in Py), 3.52 (s, 54H, CH_3 in Tab), 2.89 (s, CH_3 in DMF), 2.73 (s, CH_3 in DMF).

Preparation of $[Ag_6(Tab)_6(Bpee)_2]_2(PF_6)_{12}$·4.7CR (3). Compound **2a** (30.3 mg, 0.005 mmol) was added into 10 mL aqueous solution of CR (20.9 mg, 0.030 mmol) and the mixture stirred for 4 h in the dark at room temperature. The resulting red composite of **3** was obtained by centrifugation, washed with water and dried in vacuum. Yield: 36.8 mg (81.5%). Anal. Calcd (%) for $C_{306.4}H_{299.4}Ag_{12}F_{72}N_{48.2}Na_{9.4}O_{28.2}P_{12}S_{21.4}$: C, 40.69; H, 3.34; N, 7.46; S, 7.59; Ag, 14.31. Found: C, 40.20; H, 3.70; N, 7.28; S, 7.82; Ag, 14.32. IR (KBr disk, cm^{-1}): 1603 (m), 1489 (m), 1417 (w), 1385 (w), 1124 (m), 1042 (m), 1010 (m), 959 (w), 839 (s), 558 (s).

X-Ray Crystallographic Study. Single-crystal X-ray diffraction measurement of compound **2** was performed on a Bruker D8-Quest by using graphite monochromated Mo Kα radiation (λ = 0.7107Å). A single crystal was mounted on a glass fiber with grease at 223 K. The cell parameters refinement and data reduction were performed using the program Bruker D8 Quest with absorption correction (multi-scan) applied.[S2] The crystal structure was solved by direct method and refined with full-matrix least-squares techniques with the SHELXTL-2013 program.[S3] For **2**, two –NMe_3 groups displayed rotational disorder with the relative ratios of 0.54/0.46 and 0.66/0.34 refined for C7-C9/C7A-C9A and C43-C45/C43A-C45A, respectively. A small amount of spatially delocalized electron density in the lattice was found but acceptable refinement results could not be obtained for this electron density. The solvent contribution was then modeled using SQUEEZE in the Platon program suite.[S4] A detailed crystallographic data and structure refinement parameters of **2** are given in Table S1. Selected bond distances and angles of **2** are listed in Table S2. Crystallographic data have been deposited in the Cambridge Crystallographic Data Center (CCDC) with the number of 1900903 for **2**.

References

S1. B. V. DePamphilis, B. A. Averill, T. Herskovitz, L. Que and R. H. Holm, *J. Am. Chem. Soc*. 1974, **96**, 4159−4167.

S2. G. M. Sheldrick, *SADABS, Program for empirical absorption correction program of area detector data;* University of Göttingen, Germany, 1996.

S3. G. M. Sheldrick, *Acta Crystallogr., Sect. C: Struct. Chem.* 2015, **71**, 3–8.

S4. A. L. Spek, *J. Appl. Crystallogr.* 2003, **36**, 7–13.

Table S1 Crystal data and structure refinement parameters for **2**.

Compounds	**2**
Formula	$C_{91}H_{125}Ag_6F_{36}N_{15}O_3P_6S_6$
Formula weight	3186.45
Crystal system.	triclinic
Space group	$P\bar{1}$
a/Å	18.3280(13)
b/Å	18.8247(14)
c/Å	19.5818(15)
α/°	73.302(2)
β/°	81.107(2)
γ/°	86.840(2)
V/Å^3	6393.0(8)
D_c/(g cm^{-3})	1.655
Z	2
μ(Mo–Kα)/mm^{-1}	1.176
F(000)	3184
Total reflections	281324
Unique reflections	30413
No. observations	24603
No. parameters	1501
R_{int}	0.0417
R_1[a]	0.0723
wR_2[b]	0.1591
GOF[c]	1.116

[a] $R_1 = \Sigma||F_o|-|F_c||/\Sigma|F_o|$, $wR_2 = \{\Sigma[w(F_o^2-F_c^2)^2]/\Sigma[w(F_o^2)^2]\}^{1/2}$, GOF = $\{\Sigma[w(F_o^2-F_c^2)^2]/(n-p)\}^{1/2}$, where n is the number of reflections and p is total number of parameters refined.

Table S2 Selected bond distances (Å) and angles (°) for **2**.

Ag(1)-N(7)	2.363(5)	Ag(3)-Ag(5)#1	3.1814(7)
Ag(1)-S(2)	2.4899(16)	Ag(3)-Ag(6)	3.1981(8)
Ag(1)-N(11)	2.499(7)	Ag(4)-N(9)	2.356(5)
Ag(1)-S(3)	2.5201(16)	Ag(4)-S(6)	2.4998(14)
Ag(1)-Ag(6)	2.9269(8)	Ag(4)-S(4)	2.5761(14)
Ag(2)-S(5)	2.4302(14)	Ag(4)-S(2)	2.7196(15)
Ag(2)-S(4)	2.4382(14)	Ag(5)-N(10)#3	2.354(5)
Ag(2)-S(6)#1	2.6415(13)	Ag(5)-S(6)	2.5342(14)
Ag(2)-Ag(4)	2.9942(7)	Ag(5)-S(5)	2.5692(15)
Ag(2)-Ag(5)	3.0205(7)	Ag(5)-S(1)#1	2.7342(16)
Ag(3)-N(8)#2	2.338(5)	Ag(5)-Ag(3)#1	3.1814(7)
Ag(3)-S(2)	2.5173(15)	Ag(6)-S(1)	2.3899(17)
Ag(3)-S(1)	2.5448(17)	Ag(6)-S(3)	2.3956(16)
Ag(3)-S(5)#1	2.8428(15)	Ag(6)-S(4)	2.9358(15)
N(7)-Ag(1)-S(2)	108.51(16)	S(4)-Ag(4)-Ag(2)	51.25(3)
N(7)-Ag(1)-N(11)	90.8(2)	S(2)-Ag(4)-Ag(2)	139.93(4)
S(2)-Ag(1)-N(11)	110.1(2)	N(10)#3-Ag(5)-S(6)	106.68(14)
N(7)-Ag(1)-S(3)	107.94(16)	N(10)#3-Ag(5)-S(5)	115.33(14)
S(2)-Ag(1)-S(3)	131.29(5)	S(6)-Ag(5)-S(5)	125.72(5)
N(11)-Ag(1)-S(3)	100.56(18)	N(10)#3-Ag(5)-S(1)#1	92.73(14)
N(7)-Ag(1)-Ag(6)	121.97(15)	S(6)-Ag(5)-S(1)#1	103.52(5)
S(2)-Ag(1)-Ag(6)	81.78(4)	S(5)-Ag(5)-S(1)#1	107.04(5)
N(11)-Ag(1)-Ag(6)	140.51(18)	N(10)#3-Ag(5)-Ag(2)	118.49(14)
S(3)-Ag(1)-Ag(6)	51.52(4)	S(6)-Ag(5)-Ag(2)	79.87(3)
S(5)-Ag(2)-S(4)	156.97(5)	S(5)-Ag(5)-Ag(2)	50.76(3)
S(5)-Ag(2)-S(6)#1	103.21(5)	S(1)#1-Ag(5)-Ag(2)	146.60(4)
S(4)-Ag(2)-S(6)#1	99.19(4)	N(10)#3-Ag(5)-Ag(3)#1	122.14(14)
S(5)-Ag(2)-Ag(4)	127.71(4)	S(6)-Ag(5)-Ag(3)#1	122.59(3)
S(4)-Ag(2)-Ag(4)	55.48(3)	S(5)-Ag(5)-Ag(3)#1	58.09(3)
S(6)#1-Ag(2)-Ag(4)	92.94(3)	S(1)#1-Ag(5)-Ag(3)#1	50.26(4)
S(5)-Ag(2)-Ag(5)	54.96(4)	Ag(2)-Ag(5)-Ag(3)#1	99.472(19)

S(4)-Ag(2)-Ag(5)	127.91(4)	S(1)-Ag(6)-S(3)	161.02(6)
S(6)#1-Ag(2)-Ag(5)	95.99(3)	S(1)-Ag(6)-Ag(1)	128.73(4)
Ag(4)-Ag(2)-Ag(5)	74.301(17)	S(3)-Ag(6)-Ag(1)	55.44(4)
N(8)#2-Ag(3)-S(2)	109.93(17)	S(1)-Ag(6)-S(4)	99.82(5)
N(8)#2-Ag(3)-S(1)	117.86(16)	S(3)-Ag(6)-S(4)	98.53(5)
S(2)-Ag(3)-S(1)	118.08(5)	Ag(1)-Ag(6)-S(4)	91.13(3)
N(8)#2-Ag(3)-S(5)#1	101.56(16)	S(1)-Ag(6)-Ag(3)	51.75(4)
S(2)-Ag(3)-S(5)#1	101.81(5)	S(3)-Ag(6)-Ag(3)	129.73(4)
S(1)-Ag(3)-S(5)#1	104.55(5)	Ag(1)-Ag(6)-Ag(3)	77.219(19)
N(8)#2-Ag(3)-Ag(5)#1	131.85(17)	S(4)-Ag(6)-Ag(3)	98.27(3)
S(2)-Ag(3)-Ag(5)#1	113.41(4)	Ag(6)-S(1)-Ag(3)	80.73(5)
S(1)-Ag(3)-Ag(5)#1	55.71(4)	Ag(6)-S(1)-Ag(5)#1	125.51(6)
S(5)#1-Ag(3)-Ag(5)#1	50.10(3)	Ag(3)-S(1)-Ag(5)#1	74.02(4)
N(8)#2-Ag(3)-Ag(6)	119.12(16)	Ag(1)-S(2)-Ag(3)	99.72(5)
S(2)-Ag(3)-Ag(6)	76.05(4)	Ag(1)-S(2)-Ag(4)	110.47(5)
S(1)-Ag(3)-Ag(6)	47.52(4)	Ag(3)-S(2)-Ag(4)	105.11(5)
S(5)#1-Ag(3)-Ag(6)	137.71(3)	Ag(6)-S(3)-Ag(1)	73.03(4)
Ag(5)#1-Ag(3)-Ag(6)	91.212(19)	Ag(2)-S(4)-Ag(4)	73.27(4)
N(9)-Ag(4)-S(6)	115.02(15)	Ag(2)-S(4)-Ag(6)	140.11(5)
N(9)-Ag(4)-S(4)	104.55(14)	Ag(4)-S(4)-Ag(6)	101.87(5)
S(6)-Ag(4)-S(4)	127.40(4)	Ag(2)-S(5)-Ag(5)	74.28(4)
N(9)-Ag(4)-S(2)	95.62(14)	Ag(2)-S(5)-Ag(3)#1	127.54(5)
S(6)-Ag(4)-S(2)	111.92(5)	Ag(5)-S(5)-Ag(3)#1	71.81(4)
S(4)-Ag(4)-S(2)	96.45(4)	Ag(4)-S(6)-Ag(5)	92.37(4)
N(9)-Ag(4)-Ag(2)	113.55(14)	Ag(4)-S(6)-Ag(2)#1	122.69(5)
S(6)-Ag(4)-Ag(2)	80.93(3)	Ag(5)-S(6)-Ag(2)#1	126.63(5)

Symmetry codes for **2**: #1 2 − *x*, 1 − *y*, −1 − *z*; #2 2 − *x*, −*y*, −*z*; #3 3 − *x*, 1 − *y*, −1 − *z*.

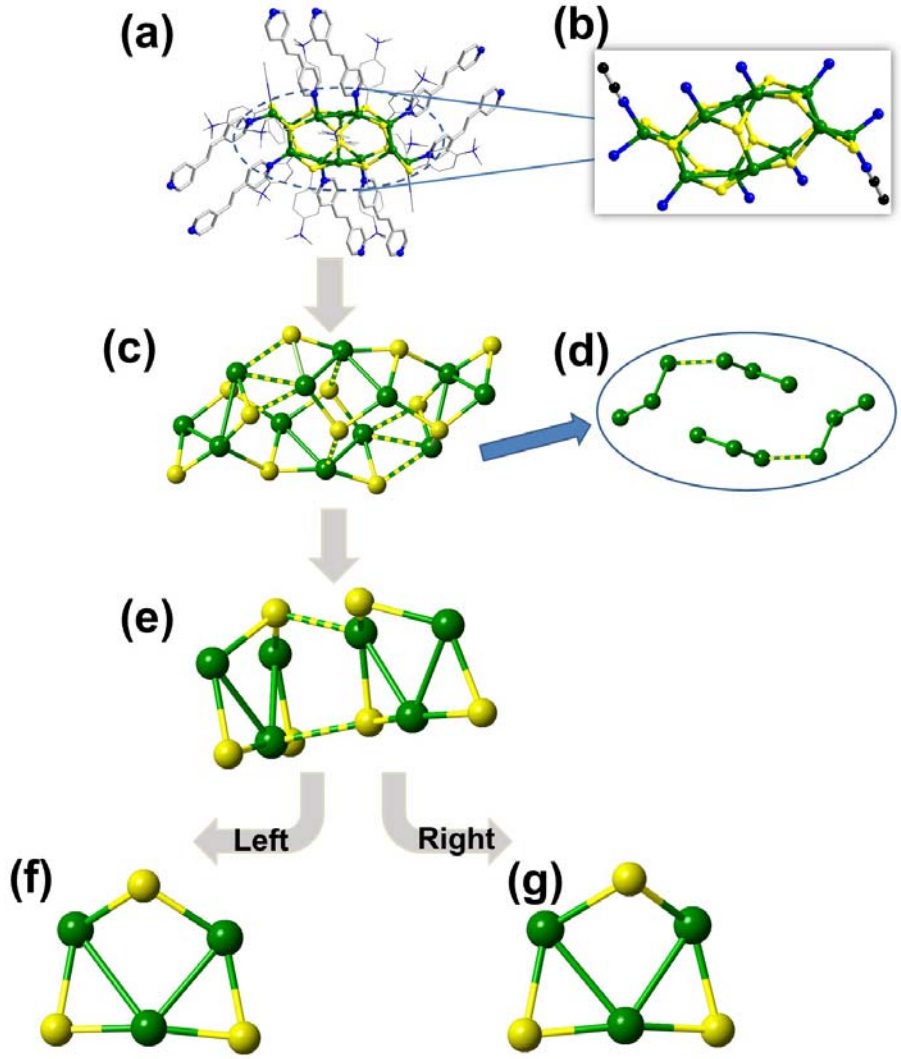

Fig. S1 The structure of the cationic cluster $[Ag_6(Tab)_6(Bpee)_2(MeCN)]_2^{12+}$ in **2** and its dissected subcomponents. (a) Overall structure; (b) Coordination environment of Ag(I); (c) Centrosymmetric $[Ag_{12}S_{12}]$ kernel; (d) Centrosymmetric Ag(I) chains; (e) $[Ag_6S_6]$ structure in asymmetric unit; (f) Pentagonal shape of the asymmetric unit (left part in e); (g) Pentagonal shape of the asymmetric unit (right part in e). All hydrogen atoms are omitted for clarity. Color codes: Ag (green), S (yellow), N (blue), and C (grey).

Additional structure description of 2.

The structure and dissection of the cationic cluster are shown in Fig. S1. The cluster SBU (Fig. S1a and S1b) can be viewed as two face-sharing prisms. From Fig. S1b, it is also evident that each of the two Ag(I) vertices at the peripheral positions are bonded by one MeCN molecule. The core structure of the cationic cluster SBU features two asymmetric units connected by Ag(I)···Ag(I) and Ag(I)···S bonds as highlighted with dual-colored bands in Fig. S1c. Two centrosymmetric Ag(I)

chains are also feasible (Fig. S1d). Each Ag(I) chain is composed of six Ag atoms. Alternatively, the core structure of the asymmetric unit (Ag_6S_6) can be viewed as constructed by a pair of similar pentagons that are nearly mutually orthogonal, and associated by a pair of Ag(I)···S bonds (Fig. S1 e–g).

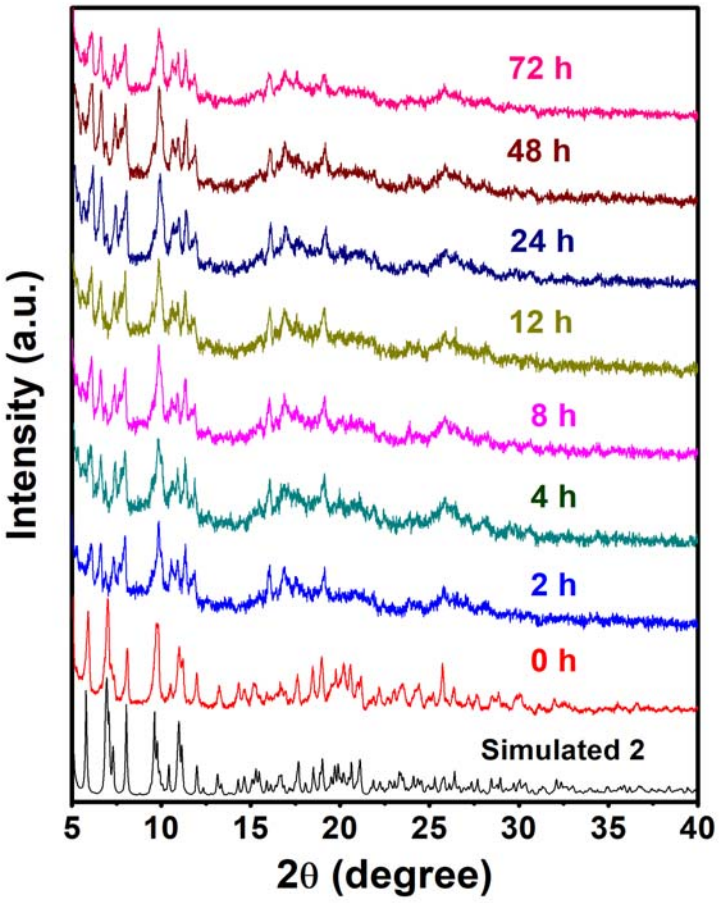

Fig. S2 The PXRD patterns of compound **2a** soaked in water for 0 h, 2 h, 4 h, 8 h, 12 h, 24 h, 48 h and 72 h coupled with that simulated **2**.

Note: Before the absorption experiment, we investigated the PXRD patterns of compound **2a** soaked in water with an extended time exposure of 72 h (Fig. S2). It was noticeable that there were some changes upon immersing **2a** in water for 2 h. Additional ^{1}H NMR spectrum (Fig. S17) of the immersed sample (2h) indicated that the DMF solvates in the lattice of **2a** had been extruded from the crystal lattice. Therefore, we presumed that a water-for-DMF process occurred that caused some notable changes of the crystal lattice and hence the varied diffraction patterns. Nevertheless, the overall structure remained robust in water.

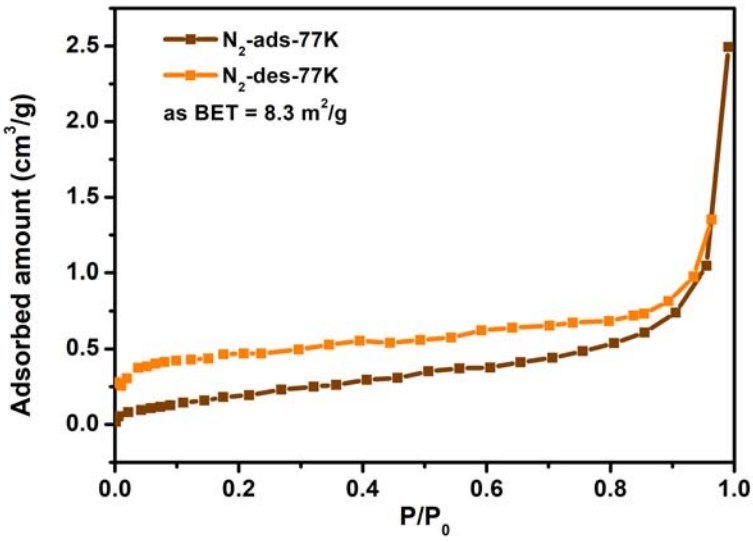

Fig. S3 Nitrogen adsorption isotherms of **2a** at 77 K, showing its absence of porosity.

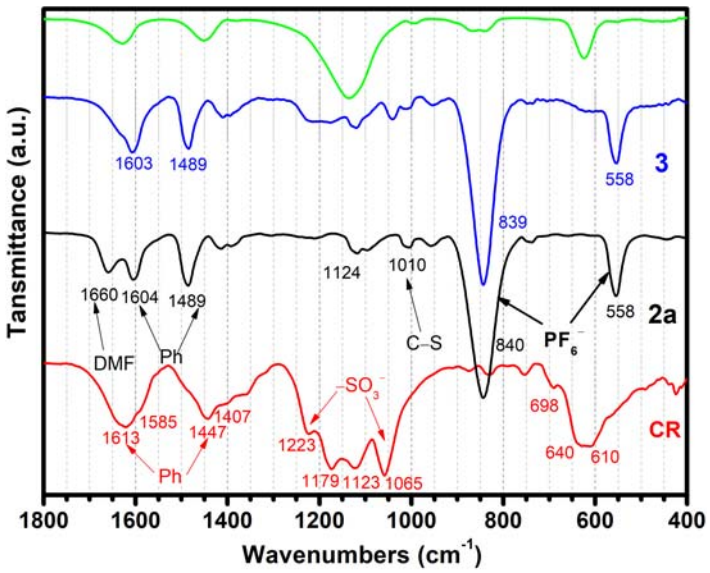

Fig. S4 The FT-IR spectra of CR (red), **2a** (black), **3** (blue) and powder collected from the residual solution of CR (green), showing differences of IR spectra among CR, **2a** and **3**, and suggesting the existence of CR in composite **3**.

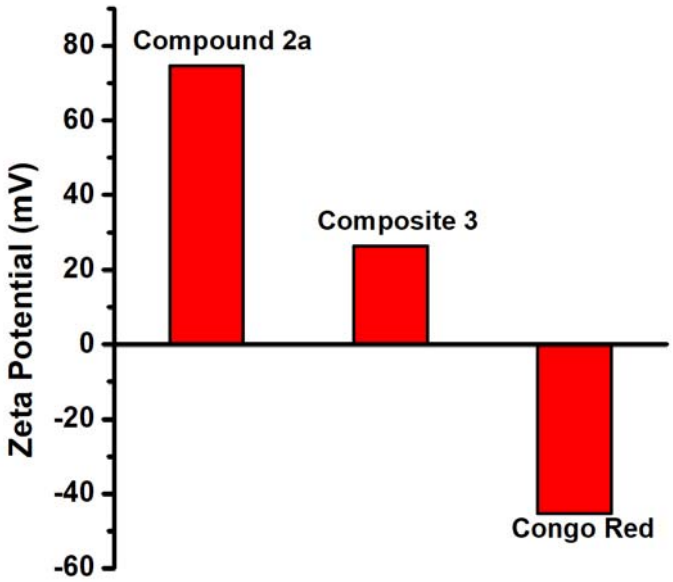

Fig. S5 Zeta potential for **2a**, **3** and CR after dispersing (or dissolving) them in water at room temperature.

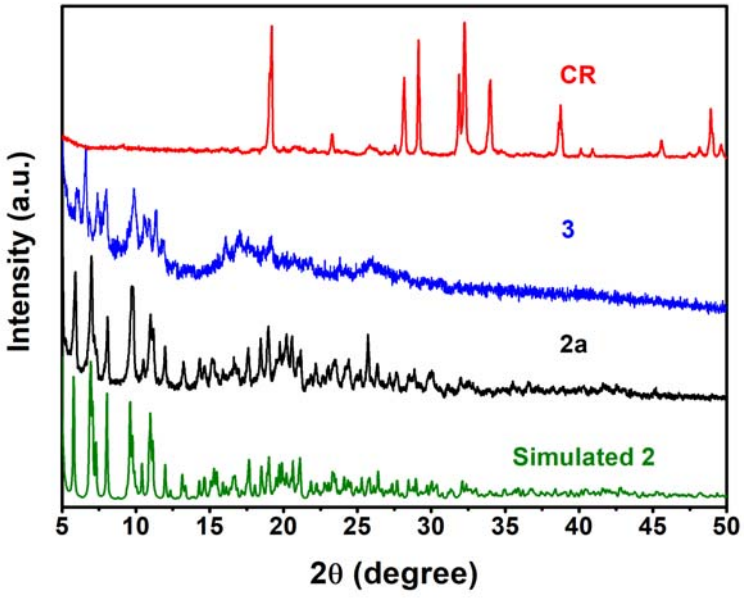

Fig. S6 The PXRD patterns of CR, **3**, **2a**, as well as that simulated from the single-crystal X-ray diffraction data of **2**.

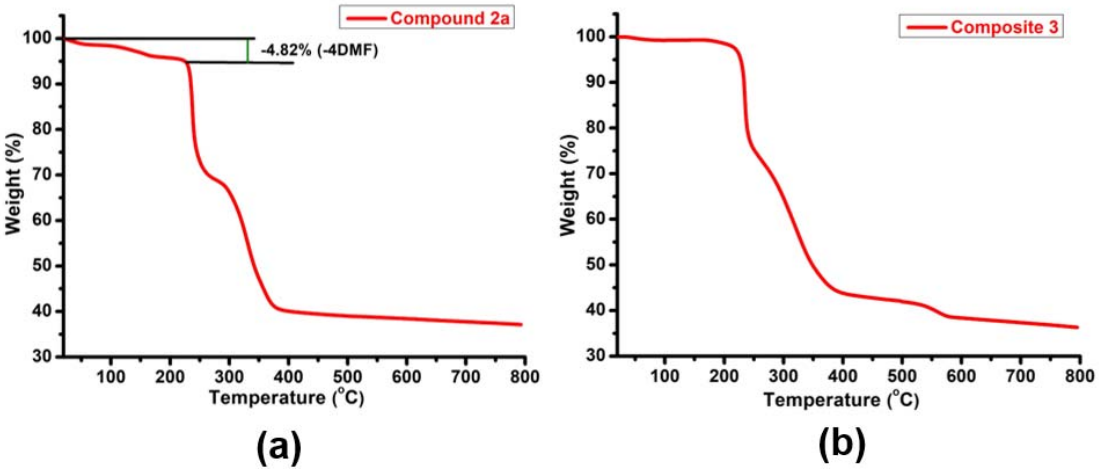

Fig. S7 The TGA curves of **2a** (a) and **3** (b), showing the different thermal decomposition of **2a** and **3**.

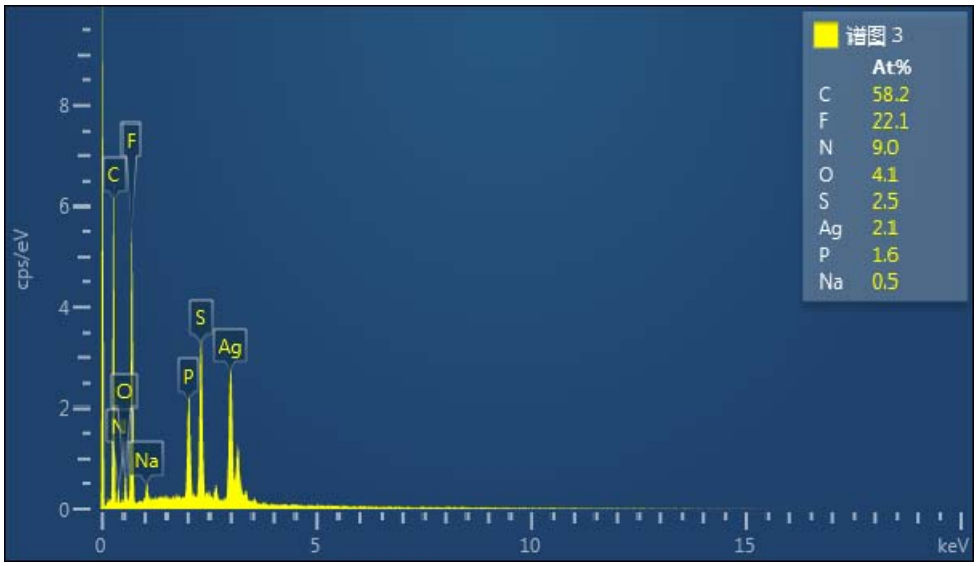

Fig. S8 EDX spectrum of composite **3**.

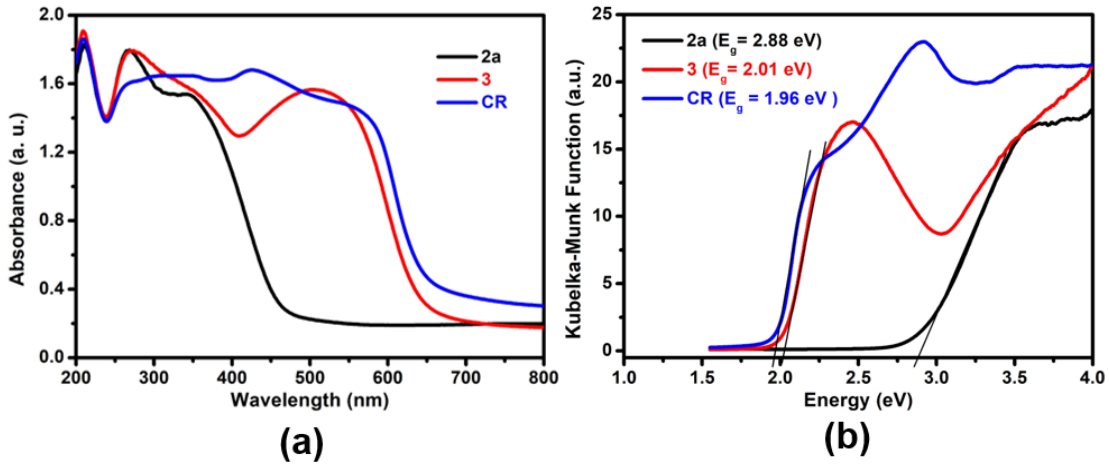

Fig. S9 (a) The solid-state UV-Vis spectra of **2a**, **3** and CR. (b) Solid-state diffusion-reflectance spectra of **2a**, **3** and CR derived from their diffuse reflectance data.

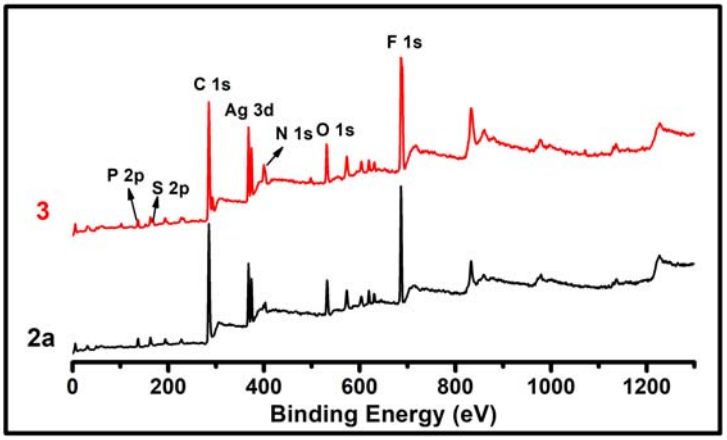

Fig. S10 XPS survey spectra of **2a** and **3**.

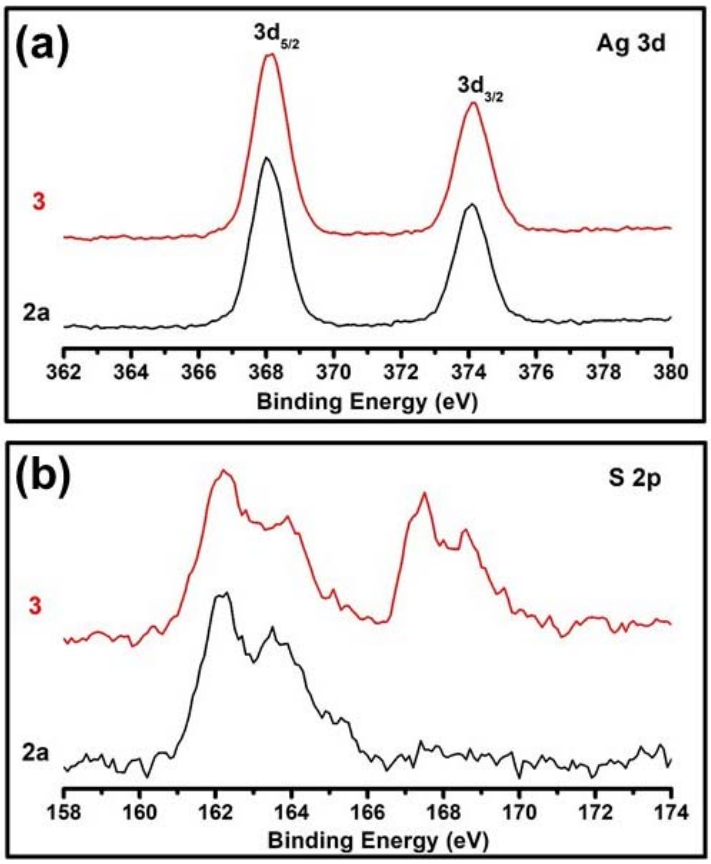

Fig. S11 High-resolution XPS spectra for Ag 3d (a), S 2p (b) of **2a** and **3.**

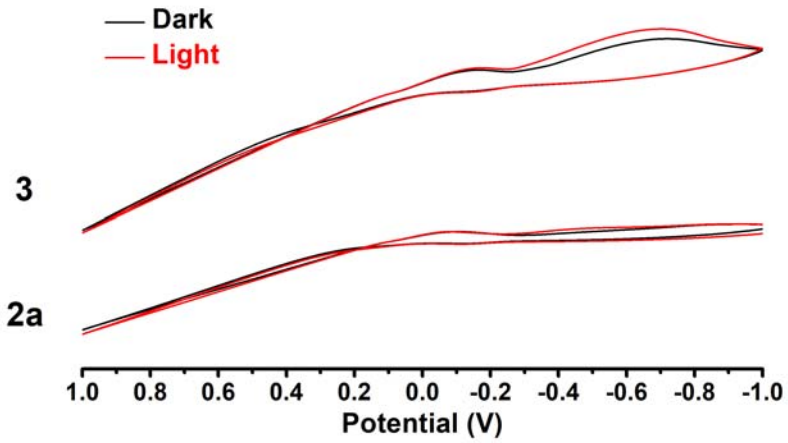

Fig. S12 Cyclic voltammograms of **2a** and **3** coated on an ITO electrode in 0.1 M Na_2SO_4 aqueous solution at a potential scan rate of 0.1 V s^{-1}.

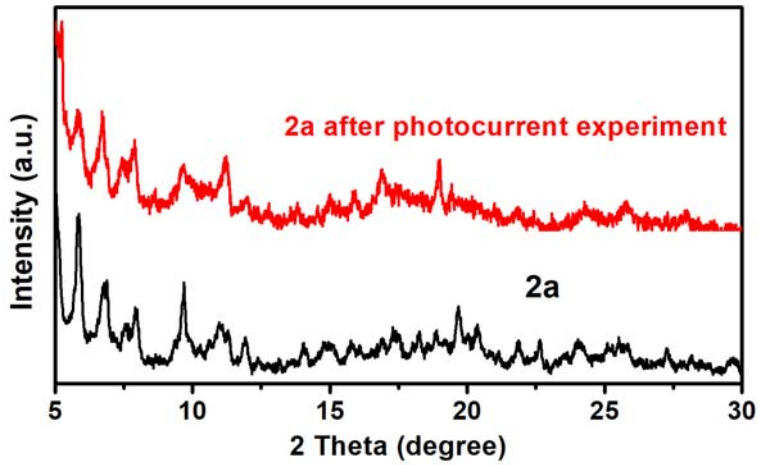

Fig. S13 The PXRD patterns of the samples scraped from the ITO electrodes after photocurrent experiments (red) and the pure samples (black) of **2a**.

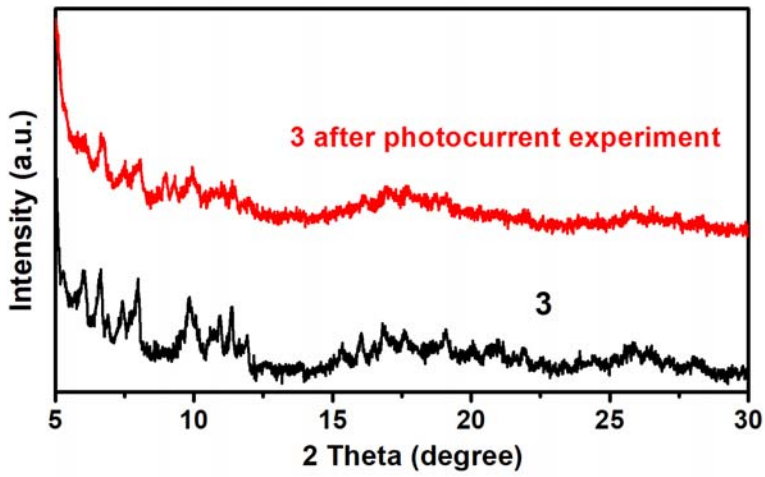

Fig. S14 The PXRD patterns of the samples scraped from the ITO electrodes after photocurrent experiments (red) and the pure samples (black) of **3**.

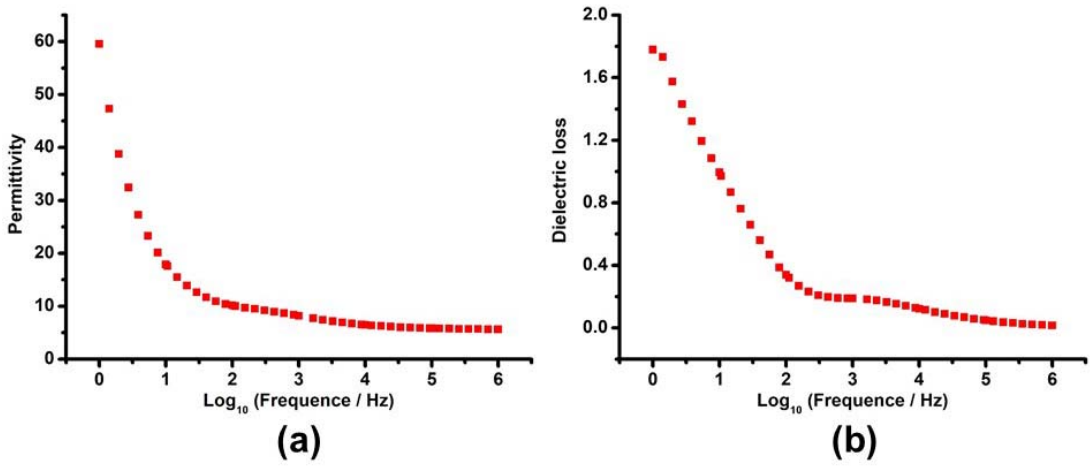

Fig. S15 (a) Frequency dependence of dielectric constants (permittivity, ε_r). (b) The frequency dependence of dielectric loss ($\varepsilon_i/\varepsilon_r$) of CR at 298 K.

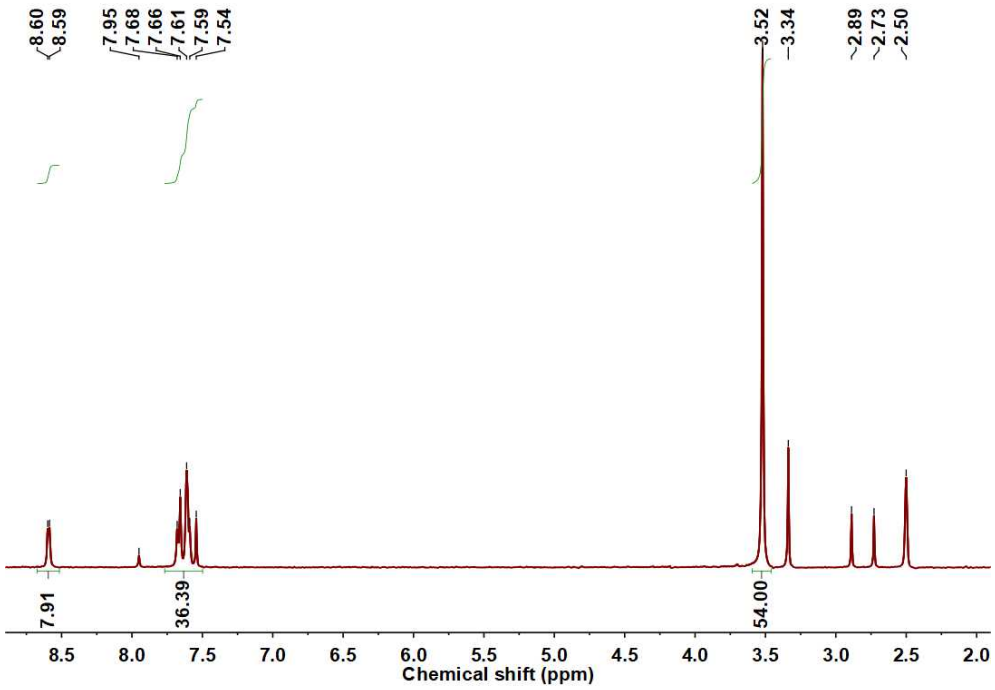

Fig. S16 The ^{1}H NMR spectrum of compound **2a** in DMSO-d_6.

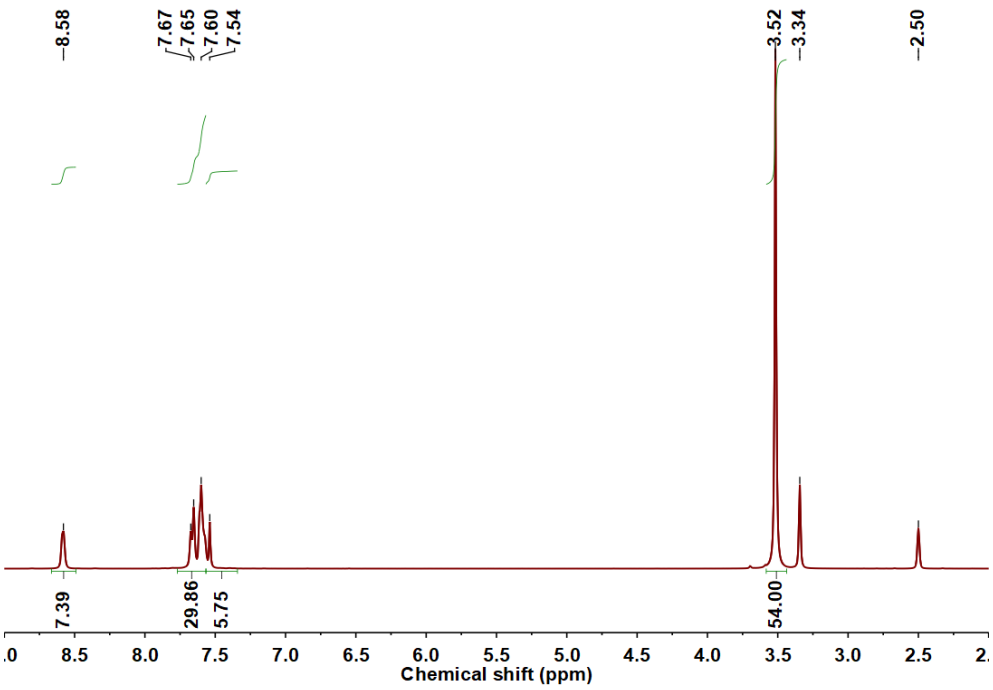

Fig. S17 The ^{1}H NMR spectrum of the sample after immersing **2a** in water for 2 h in DMSO-d_6.

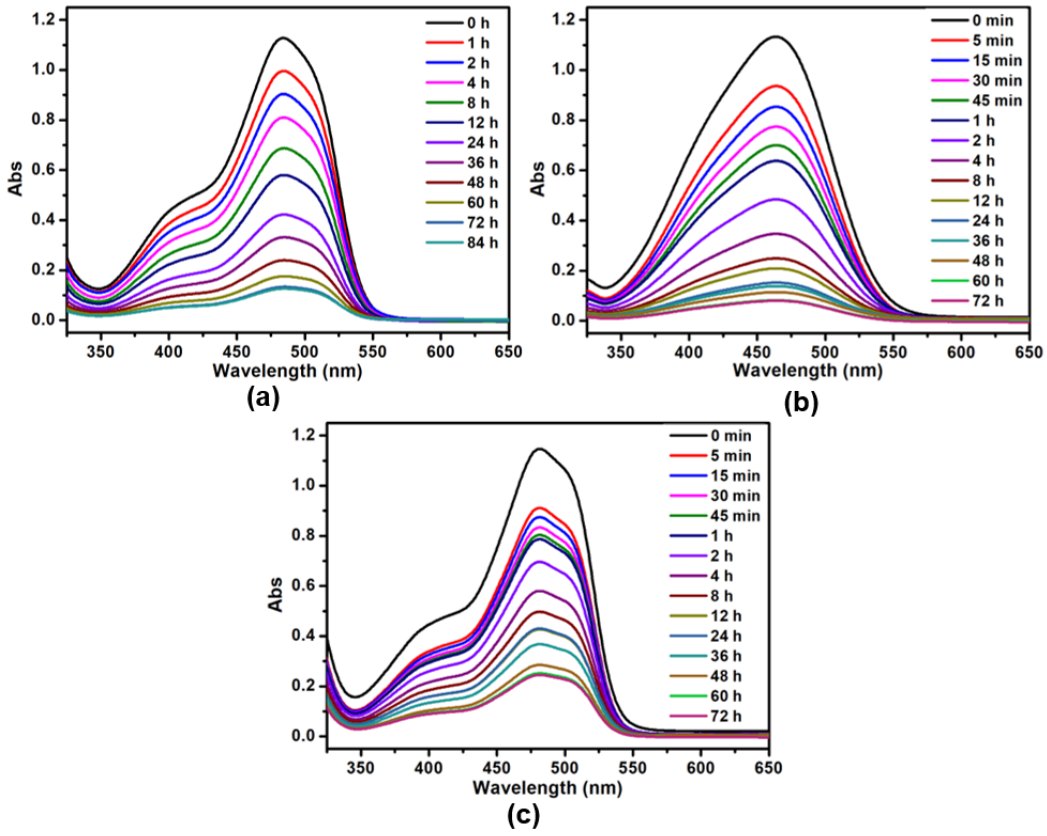

Fig. S18 Absorption spectra of the anionic dye solutions including OII (a), MO (b) and SY (c) after mixing with **2a** at different time intervals.

Note: For a quantitative study, a well-grounded powder of **2a** (0.005 mmol) was added into the aqueous solution of each negatively charged dye (3 mM, 10 mL) with continuous stirring at room temperature in the dark, with the uptake process monitored by UV-Vis spectroscopy. The resulting insoluble powders were isolated from the aqueous solutions of OII, MO and SY by centrifugation, washed with water and dried in vacuum. And the above three products were named as composite **4**, **5** and **6**, respectively. From the comparison of their IR spectra, it can be inferred that an anion exchange between PF_6^- and anion in each dye took place during their uptake process. This phenomenon further explained why compound **2a** had a better uptake capacity and a faster uptake rate for CR compared to the other dyes.

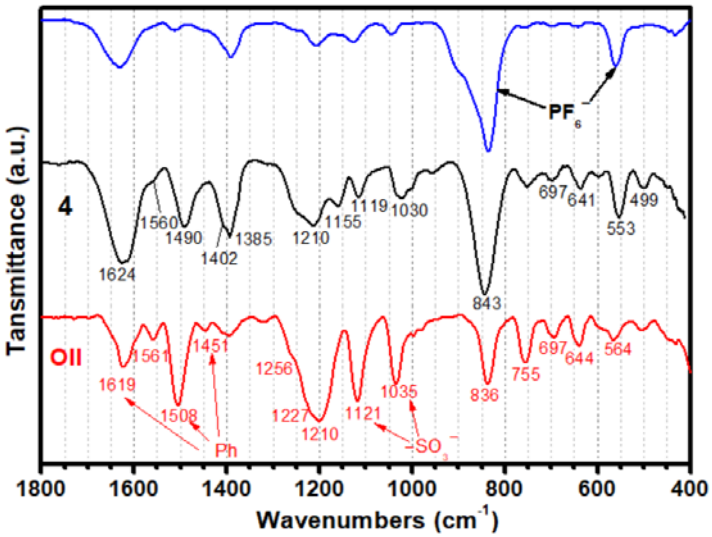

Fig. S19 IR spectra of OII (red), **4** (black) and powder collected from the residual solution of OII (blue), suggesting the existence of anion exchange during the consumption of OII.

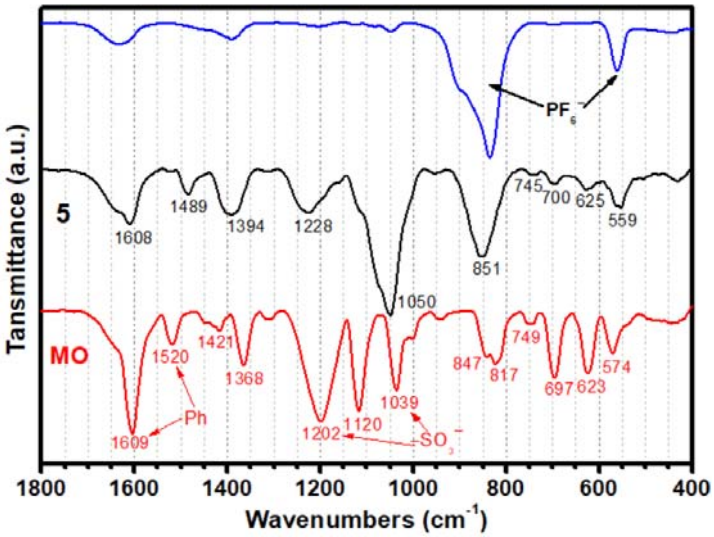

Fig. S20 The FT-IR spectra of MO (red), **5** (black) and powder collected from the residual solution of MO (blue), suggesting the existence of anion exchange during the consumption of MO.

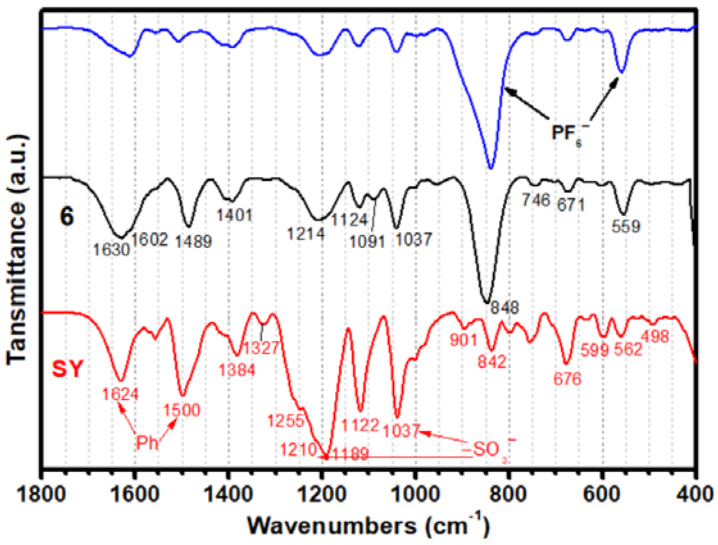

Fig. S21 The FT-IR spectra of SY (red), **6** (black) and powder collected from the residual solution of SY (blue), suggesting the existence of anion exchange during the consumption of SY.

Chart 1 The structures of the anionic dyes used in absorption experiments.